Viscoplastic drop impact on thin films

Samya Sen, Anthony G. Morales, Randy H. Ewoldt[1]
Department of Mechanical Science and Engineering
University of Illinois at Urbana-Champaign, Urbana, IL 61801, USA

Supplementary Information

1 Choice of rheological model

The steady shear data for Laponite and Carbopol have been fit to three generalised Newtonian fluid (GNF) models. The simplest model is the Bingham [2],

$$\sigma = \sigma_{\mathrm{y}} + \eta_\infty \dot{\gamma}, \tag{1}$$

where σ_{y} is the shear yield stress and η_∞ is the Bingham plastic viscosity. The Herschel-Bulkley model usually fits data for clays and gels better, but does not have a finite viscosity at very high rates. For this, one can use a generalised Herschel-Bulkley model,

$$\sigma = \sigma_{\mathrm{y}} + K\dot{\gamma}^n + \eta_\infty \dot{\gamma}, \tag{2}$$

where K and n are the Herschel-Bulkley consistency and flow indices respectively. This model has a finite viscosity at high shear rates, but fits data at intermediate and low shear rates better than Bingham. But fits to this model can lead to uncertainties in the parameters since one may not have enough data to fit four free parameters. For this, the flow index, n, is often kept fixed at 0.5, and the other three parameters are allowed to be free in the fit. This is also physical, and the $n = 0.5$ scaling is found to be close to the exponent for most soft particle glasses and gels as mentioned in the manuscript. This modified form of the generalised Herschel-Bulkley model is

$$\sigma = \sigma_{\mathrm{y}} + K\dot{\gamma}^{0.5} + \eta_\infty \dot{\gamma}, \tag{3}$$

where $n = 0.5$ is fixed.

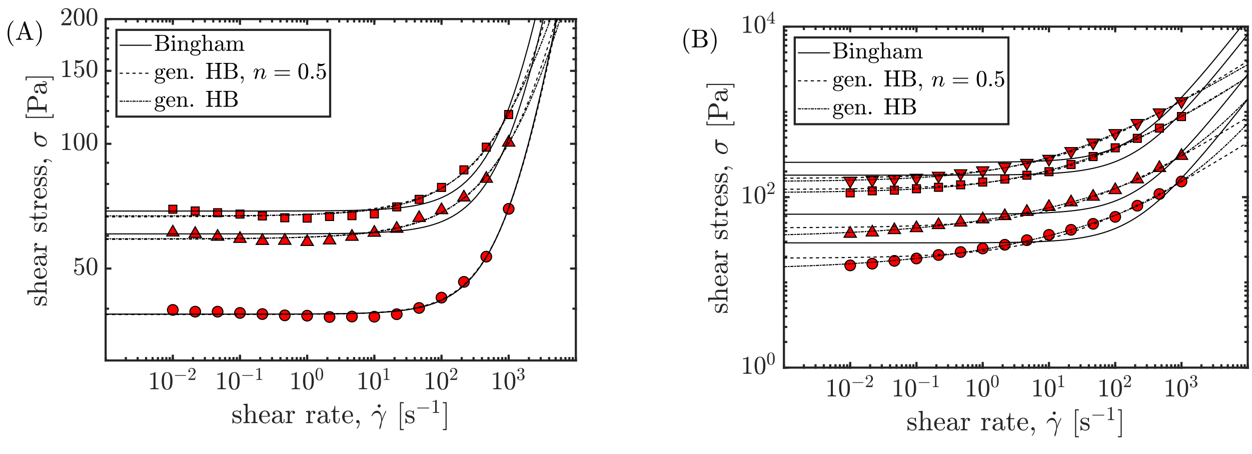

Figure S1: Steady-state flow curves for the Laponite and Carbopol concentrations used, fit to each model. (A) Data for Laponite, (B) data for Carbopol.

In order to determine which model to use in our dimensionless group, one has to choose the most credible model. Simply using the one with the smallest residual is not the best practice, and one must use more refined metrics of model selection. We use an approximate Bayesian inference criterion (BIC) to do this [4]. The BIC is defined as

$$\mathrm{BIC} = n + n\ln 2\pi + n\ln\frac{\mathrm{RSS}}{n} + p\ln n, \tag{4}$$

[1]author to whom all correspondence should be addressed; ewoldt@illinois.edu

where n is the length of the data set (in our case, the number of shear rates the data was collected at), RSS is the residual sum of squares of the fit obtained during optimisation, and p is the number of parameters in the model used. The smaller the RSS, the smaller the BIC, and the better the fit. But as one increases the number of fit parameters, while the raw fit improves, thus decreasing the RSS, the penalty term, $p \ln n$ also increases with p, and thus BIC increases, thus deteriorating the fit quality. We use the most credible model - the one which has not the smallest RSS, but the smallest BIC. Fig. S2 plots the BIC values for all formulations used vs. the model chosen to fit the data.

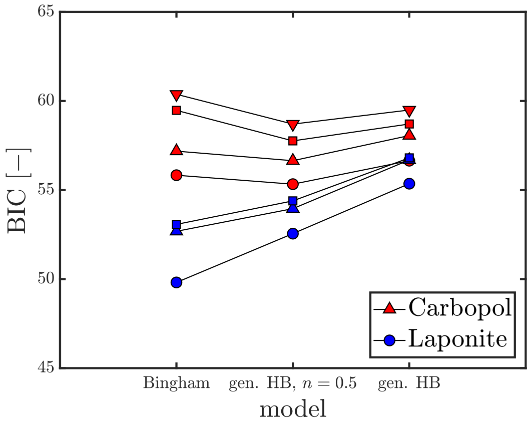

Figure S2: BIC versus the model used for each formulation used in this work.

As we can clearly see, the generalised HB model with $n = 0.5$ is the most credible model for Carbopol, while it is the second best Laponite. We therefore choose to use this model for defining the flow stress term in our dimensionless group, which is given as

$$\mathrm{IF}\left(\frac{D}{t}\right) \equiv \frac{\rho V^2}{\sigma_\mathrm{y} + K\,(V/t)^{0.5} + \eta_\infty V/t}\left(\frac{D}{t}\right). \tag{5}$$

This dimensionless group is used to plot the regime maps in the paper. The fit parameters obtained for each model from the flow data are also shown in tables S1, S2.

Bingham		gen. HB, $n = 0.5$			gen. HB			
σ_y [Pa]	$\eta_\infty \times 10^2$ [Pa·s]	σ_y [Pa]	$K \times 10^2$ [Pa·s$^{0.5}$]	$\eta_\infty \times 10^2$ [Pa·s]	σ_y [Pa]	$K \times 10^2$ [Pa·s^n]	n [−]	$\eta_\infty \times 10^2$ [Pa·s]
38.8 ± 0.4	3.1 ± 1.3	38.7 ± 0.5	3.7 ± 12.5	2.9 ± 0.4	38.8 ± 1.8	2.3 ± 184.6	0.00 ± 1.12	3.1 ± 0.2
60.6 ± 1.5	4.3 ± 0.5	58.8 ± 1.0	78.4 ± 25.2	1.7 ± 0.9	59.0 ± 1.3	54.3 ± 90.5	0.59 ± 0.46	0.8 ± 5.4
70.6 ± 1.8	5.3 ± 0.6	66.6 ± 1.2	94.5 ± 0.3	2.2 ± 1.1	67.0 ± 1.3	51.6 ± 72.2	0.66 ± 0.44	0.0 ± 8.9

Table S1: Rheological fit parameters for Laponite with uncertainties corresponding to 95% confidence bounds.

Bingham		gen. HB, $n = 0.5$			gen. HB			
σ_y [Pa]	$\eta_\infty \times 10^2$ [Pa·s]	σ_y [Pa]	K [Pa·s$^{0.5}$]	$\eta_\infty \times 10^2$ [Pa·s]	σ_y [Pa]	K [Pa·s^n]	n [−]	$\eta_\infty \times 10^2$ [Pa·s]
29.1 ± 7.2	13.8 ± 2.6	19.2 ± 1.9	4.2 ± 0.5	0.0 ± 1.7	14.0 ± 2.7	10.3 ± 2.9	0.31 ± 0.06	5.5 ± 1.3
63.0 ± 14.2	27.0 ± 5.0	43.6 ± 3.6	8.2 ± 1.0	0.0 ± 3.3	33.9 ± 5.2	19.6 ± 5.8	0.31 ± 0.06	10.5 ± 2.7
181.2 ± 44.6	79.2 ± 15.8	122.9 ± 6.3	24.3 ± 1.7	0.0 ± 5.8	112.7 ± 4.6	33.4 ± 4.4	0.44 ± 0.03	4.7 ± 6.6
256.0 ± 70.1	122.3 ± 24.8	165.7 ± 10.2	37.7 ± 2.7	0.0 ± 9.3	152.2 ± 6.5	48.4 ± 6.1	0.46 ± 0.03	0.0 ± 10.6

Table S2: Rheological fit parameters for Carbopol with uncertainties corresponding to 95% confidence bounds.

2 Repeat measurements for steady flow data

Presence of wall slip in rheological measurements done with parallel plate geometries is quite well-known. Complex fluids, especially yield-stress fluids, are not free from this error. Therefore, tests are repeated with different gaps, and any significant disagreement between data for different gaps is an indicator of wall slip [3].

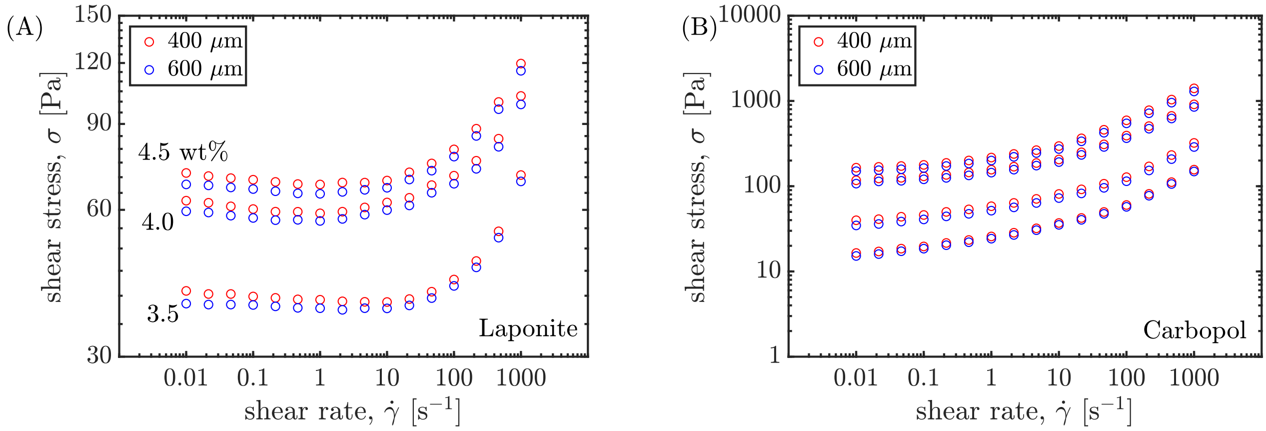

Figure S3: Steady-state flow curves for the Laponite and Carbopol concentrations used, showing repeats at two different gaps. (A) Data for Laponite, (B) data for Carbopol.

Laponite RD is known to adhere quite well with stainless steel, but repeats were done nevertheless to check for any possible inaccuracies. Two different gaps for the parallel plate geometry were used: 400 and 600 μm. The results of the repeats are shown in Fig. S3. As we can see, the two data sets agree quite well, with the maximum difference between a pair of points being less than 10%. So there was very little slip during the measurements, if any, and the data used in the paper was an average of the two data sets shown here. Similar trends were observed with Carbopol data.

3 Experimental and geometrical parameter space explored

A range of experimental parameters (material and geometric) was investigated in this work. The 3-D space of geometric parameters is shown in Fig. S4. Each such space was tested with each concentration of Laponite RD, with at least two repeat measurements for each test to confirm the outcome of the impact event.

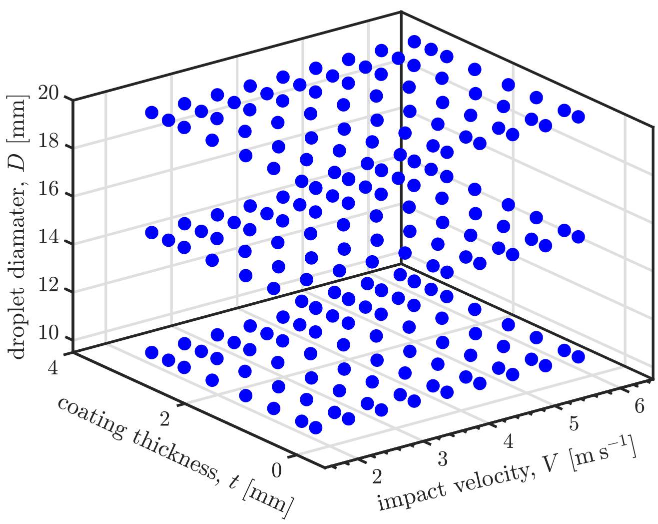

Figure S4: Experimental parameter space. The range of geometric parameters explored for a given concentration (wt%) in the study is shown here.

4 Typical impact event types observed

The regime maps used to rationalise impact events were plotted based on the kind of impact event that occurred, which were deemed to be of five types [1]. These are shown in Fig. S5. For the representative impacts shown here, the exact experimental conditions for which these were obtained are tabulated in table 4.

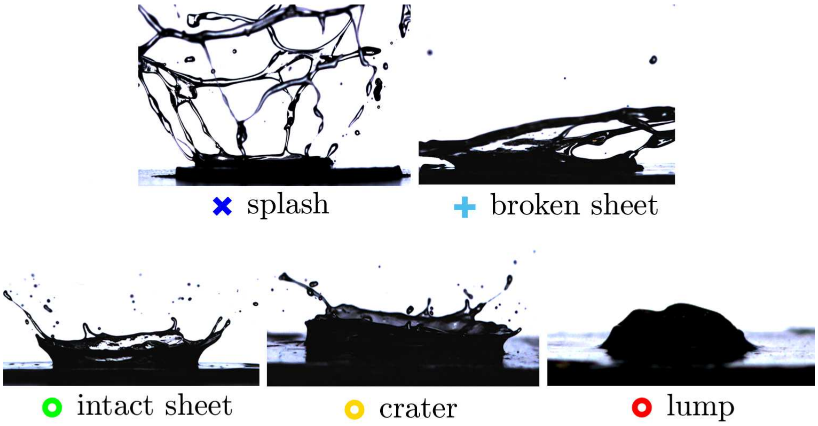

Figure S5: Various impact events observed during experiments. The impact event types shown here are used as references for judging the type of impact. A compilation of supplementary videos that illustrate these impact types can be found here.

impact type	wt%	V (m s^{-1})	D (mm)	t (mm)
splash	3.5	5.0	15	3.18
broken sheet	3.5	3.0	15	2.88
intact sheet	3.5	2.4	15	2.88
crater	4.0	2.0	20	3.18
lump	4.0	2.0	10	3.18

Table S3: Experimental conditions for the representative examples shown in Fig. S5.

The specific symbols used to label the impact types as seen in Fig. S5 have been maintained across all regime maps, without exception. The boundary of splash-stick behaviour can be chosen to be that between any pair of adjacent event types.

5 Plots of IF(D/t) vs. Bingham number, Bn, and alternate choices of regime boundaries

The Bingham number is defined as the ratio of plastic to flow components of stress. It can thus be defined, for the generalised Herschel-Bulkley model used to plot the regime maps, as

$$\mathrm{Bn} \equiv \frac{\sigma_{\mathrm{y}}}{K\,(V/t)^{0.5} + \eta_\infty V/t}, \tag{6}$$

where K and η_∞ are model parameters from fitting steady flow curves to the generalised Herschel-Bulkley model with $n = 0.5$ (eq. 3).

The plots of IF$\,(D/t)$ vs. Bn are shown in fig. S6. The regime boundary of interest, that between intact and broken sheet types, happens to lie around Bn ~ 1. So the effect of both the plastic component of stress, σ_{y}, and the flow or rate-dependent component, due to K and η_∞, are significant in the dimensionless grouping. Yield stress plays an equally, if not more, important role, in the transition from stick to splash. One can also look at other regime boundaries, where the Bn is even larger, and the effects of the yield stress dominate even more over the rate-dependent stresses.

The boundary between splash and stick has been chosen to be that between broken sheet and intact sheet impact types. The values of C obtained are unique to this choice. It is expected that the value of C for transition from one

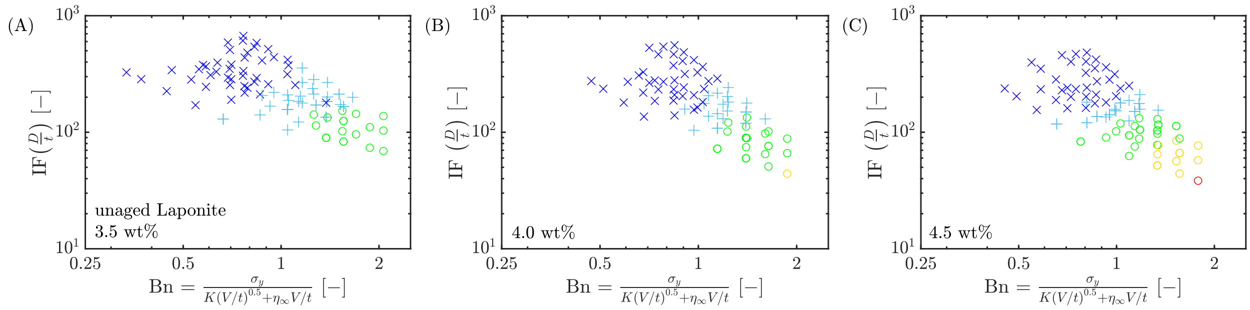

Figure S6: Plots of IF(D/t) vs. Bingham number for all concentrations of Laponite.

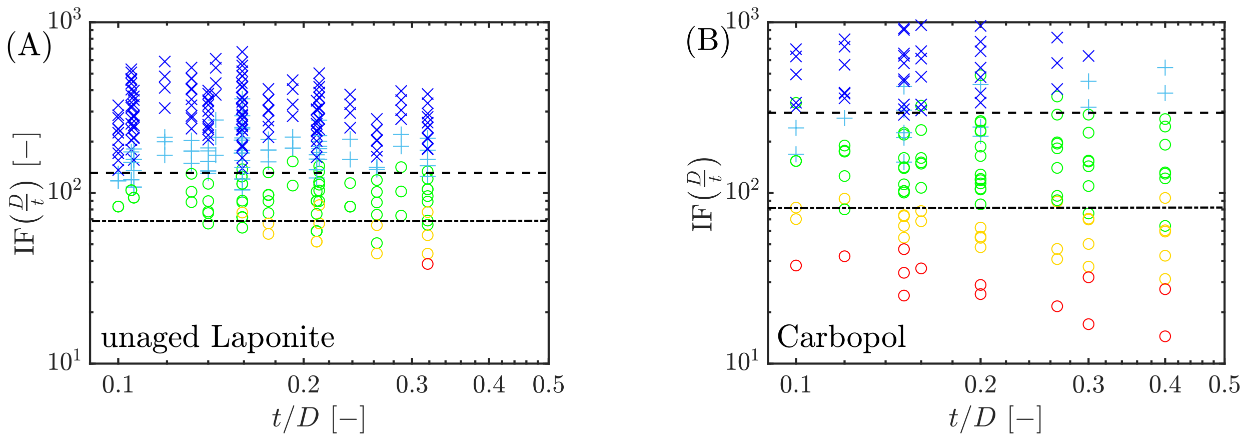

Figure S7: Comparison of different regime boundaries for (A) unaged Laponite and (B) Carbopol [1]. The value of C can be chosen to represent the separation between different impact events. These can be broken sheet - intact sheet (dashed) or intact sheet - crater (dash-dotted). Different values of C are obtained for each case, although values for the same boundary are of the same order for Carbopol and Laponite. The results have been documented in table 5.

regime to another shall depend on the choice of the pair of impact types deemed representative of stick-splash. Say we instead chose the boundary between intact sheet - crater. We can obtain the values of C for this case similar to the way we did earlier. The two such regime boundaries are shown for both Laponite and Carbopol in Fig. S7. Note that other boundaries are not so clear, especially for Laponite. Although one can observe a distinct boundary between crater - lump for Carbopol, we do not have sufficient data points for Laponite to make this observation.

material	C (broken-intact sheet)	C (intact sheet-crater)
unaged Laponite	131 ± 26	68 ± 15
Carbopol	295 ± 46	81 ± 10

Table S4: Table showing the change in critical value of C with the choice in regime boundary to be fit to.

The different values of C than can be obtained for each of these two choices are tabulated in table 5. But as noted in the manuscript as well, for applications that can benefit from our results, to be specific, spray coating, fire suppression, etc., the most important and relevant transition in behaviour is that between intact and broken sheet types. So we have kept this the focus of all analysis in the main paper, but we also provide some information of other possible choices. As we can see, the values are vastly different between the different choices, but are of the same order for a given choice between Carbopol and Laponite. This reiterates the universality of the non-dimensionalisation used to plot the regime maps, at least for the two materials used in this work.

6 Dependence of IF and C on the steady flow data

6.1 Dependence on range of flow data

Here, we plot the regime maps using flow data with a narrower range of shear rates, and define IF based on the Bingham model. The flow curve in fig. S8 show the data and Bingham fits for the shear rate range of $0.1 - 100\ \mathrm{s}^{-1}$. The regime maps defined using parameters from these fits are shown in fig. S9.

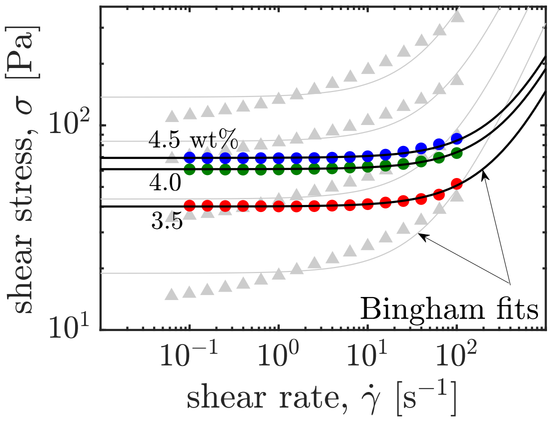

Figure S8: Flow curve using a narrower range of shear rates.

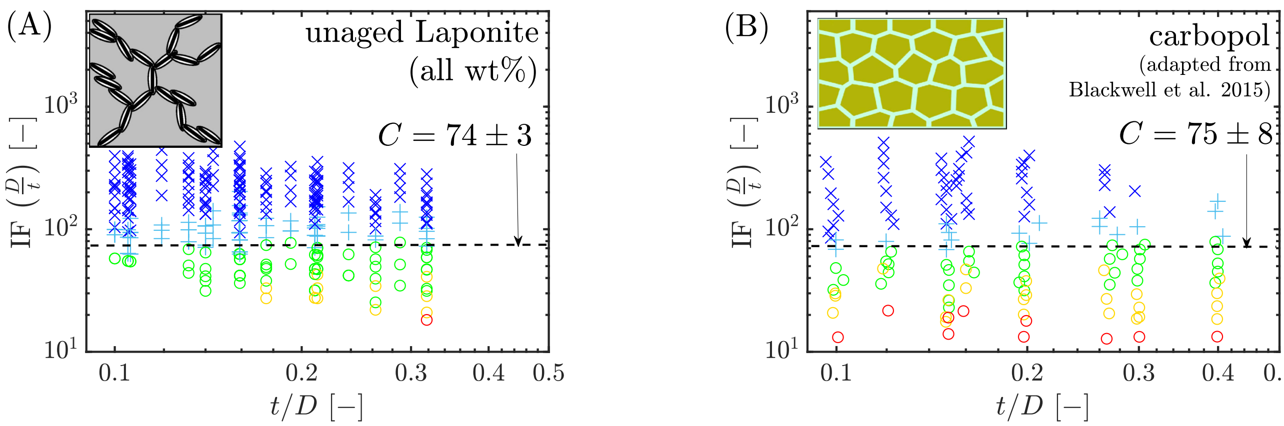

Figure S9: Comparison of regime maps plotted using narrower range of shear rates in flow curves.

As we can see, the values of C for Laponite and Carbopol are 74 ± 3 and 75 ± 8 respectively instead of 118 ± 24 and 205 ± 50 from the wider shear rate data, shown in fig. S10 (using Bingham model for both). It is pure coincidence that the C values almost matched for the two fluids, which we now know is not universal; it actually depends heavily on the range of data and related uncertainties, and, as shown next, on the choice of the rheological model.

6.2 Dependence on choice of rheological model

Here, we plot the regime maps using the dimensionless group defined based on each of the three rheological models the steady flow data was fit to. The group based on the Bingham model is

$$\mathrm{M1} \equiv \mathrm{IF}\left(\frac{D}{t}\right) = \frac{\rho V^2}{\sigma_\mathrm{y} + \eta_\infty V/t}\left(\frac{D}{t}\right). \tag{7}$$

The group based on the generalised Herschel-Bulkley model is.

$$\mathrm{M2} \equiv \mathrm{IF}\left(\frac{D}{t}\right) = \frac{\rho V^2}{\sigma_\mathrm{y} + K\left(V/t\right)^n + \eta_\infty V/t}\left(\frac{D}{t}\right), \tag{8}$$

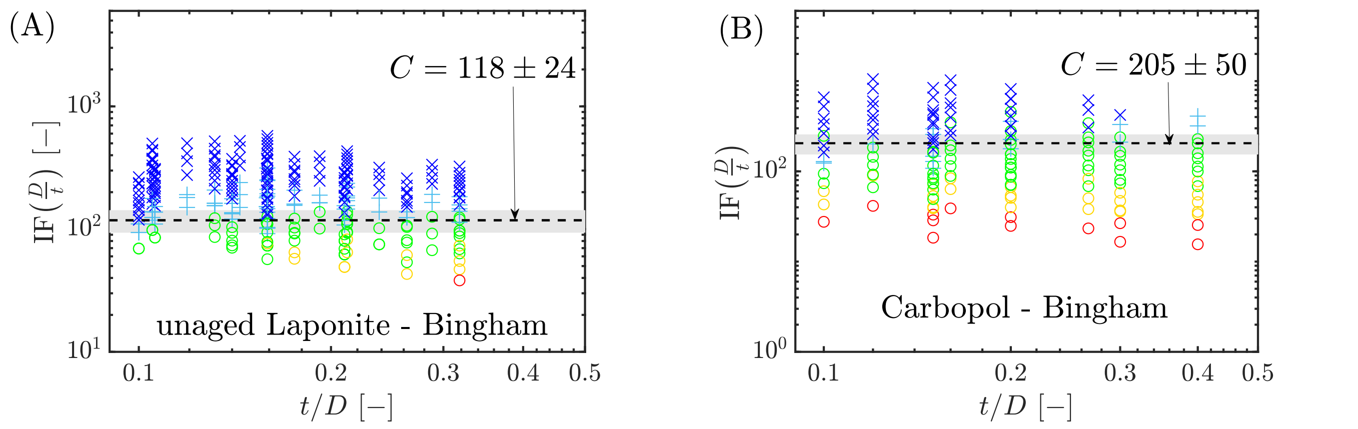

Figure S10: M1 plots: comparison of regime maps for (A) Laponite, and (B) Carbopol, plotted using the Bingham model.

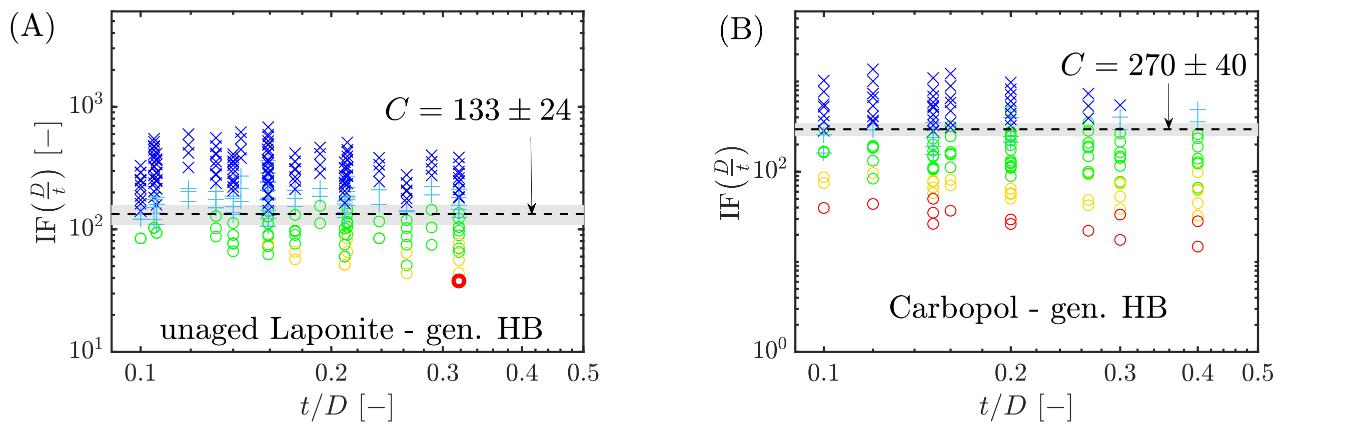

Figure S11: M2 plots: comparison of regime maps for (A) Laponite, and (B) Carbopol, plotted using the generalised Herschel-Bulkley model.

The group using the generalised Herschel-Bulkley with $n = 0.5$ is

$$\mathrm{M3} \equiv \mathrm{IF}\left(\frac{D}{t}\right) = \frac{\rho V^2}{\sigma_{\mathrm{y}} + K\,(V/t)^{0.5} + \eta_\infty V/t}\left(\frac{D}{t}\right). \tag{9}$$

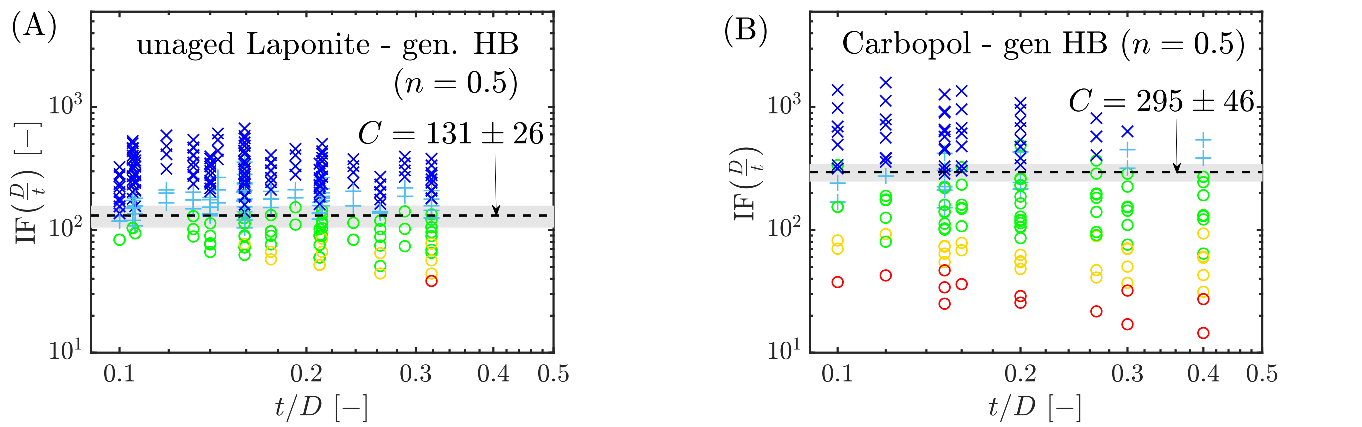

Figure S12: M2 plots: comparison of regime maps for (A) Laponite, and (B) Carbopol, plotted using the generalised Herschel-Bulkley model with $n = 0.5$.

The regime maps for both Laponite and Carbopol using each of these are shown in figs. S10, S12, S11. As we can see from the plots, the critical values of C for each material is largely independent of the choice of rheological model, although the exact values do vary with the model. When comparing the values of C for Laponite and Carbopol, we see that they are of the same order of magnitude, no matter what model is used.

7 Case study: drop impacts with Bentonite clay

As a starting point for extending this study, we performed some one-off tests with Bentonite, a more "usual" clay used in drop impact studies. All samples were prepared and tested following the procedure laid out in the paper. We impacted $D = 15$ mm diameter drops of 13 wt% Bentonite onto $t = 2.63$ mm thick coatings, at varying velocities, V.

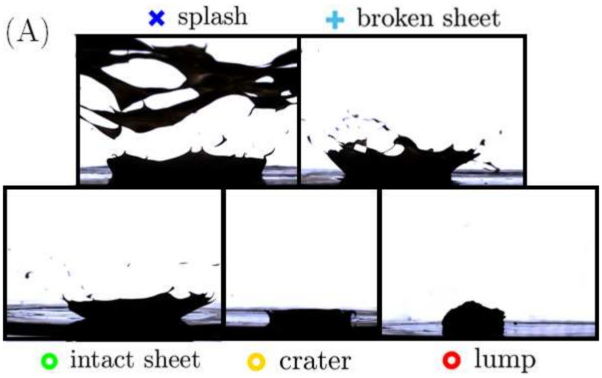

Figure S13: Various impact events observed during experiments. The impact event types shown here are used as references for judging the type of impact. A compilation of supplementary videos that illustrate these impact types can be found here.

The steady shear rheological data for the Bentonite suspension used is shown in fig. S14 (A). Also shown are fits to the three rheological models used to fit Laponite and Carbopol data. We use the fit parameters from the generalised Herschel-Bulkley model with $n = 0.5$ to plot the drop impact results for Bentonite on top of those for Laponite, also shown in fig. S14 (B).

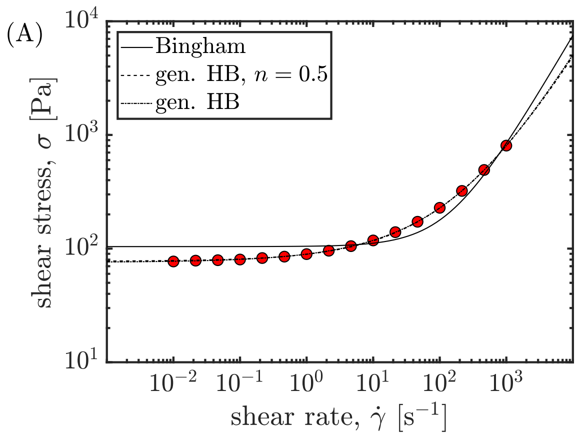

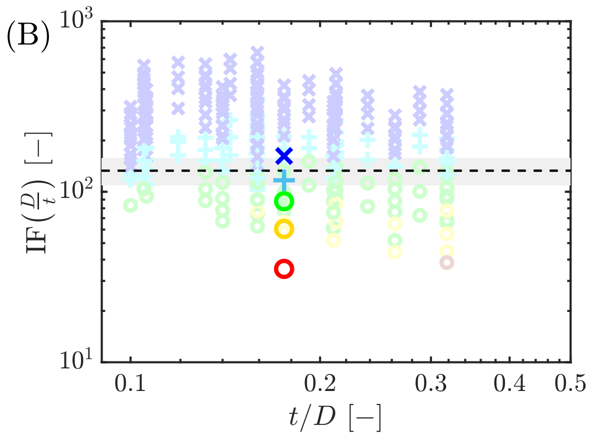

Figure S14: Data for Bentonite. (A) Steady shear rheological data for 13 wt% Bentonite, fit to all three models. (B) One-off drop impact tests with Bentonite plotted using IF(D/t), co-plotted with results for Laponite.

The flow curve of Bentonite looks similar to that of Laponite, which makes sense is a way since both are clays. The rheological parameters obtained for fitting this data to the three models used earlier are shown in table S5.

The five drop impact tests, shown in fig. S13, were done to see each of the characteristic typical behaviours seen for the other fluids. The co-plots with Laponite data provide good evidence of this dimensionless group being more universal than at first sight. We see that the five impact types more or less lie where they are predicted for Laponite. The broken sheet type is slightly below the transition boundary between stick and splash, although it is still within the error window. These tests provide additional evidence for the validity of this group, and further studies with different yield-stress fluids should only strengthen the robustness of this scaling.

Bingham		gen. HB, $n = 0.5$			gen. HB			
σ_y [Pa]	η_∞ [Pa·s]	σ_y [Pa]	K [Pa·s$^{0.5}$]	η_∞ [Pa·s]	σ_y [Pa]	K [Pa·s^n]	n [−]	η_∞ [Pa·s]
104.2 ± 19.1	0.74 ± 0.07	77.4 ± 0.9	11.3 ± 0.2	0.37 ± 0.01	75.8 ± 0.5	13.3 ± 0.5	0.46 ± 0.01	0.41 ± 0.01

Table S5: Rheological fit parameters for Bentonite with uncertainties corresponding to 95% confidence bounds.

8 Full regime maps with all film thicknesses

The data in the lower ranges of t/D were omitted for two main reasons: (i) our experiments produced a sparse data set for the thinnest films (for t/D values smaller than indicated by the red line in the plots). Any estimates of a regime boundary would not be reliable, and, (ii) we are focusing on the thin film regime only. Even thinner films may push us into the very thin film regime where properties of the substrate (roughness, wettability, etc.) become very important [5], so must be included in the modeling. This case, along with very deep pools, need their own separate study.

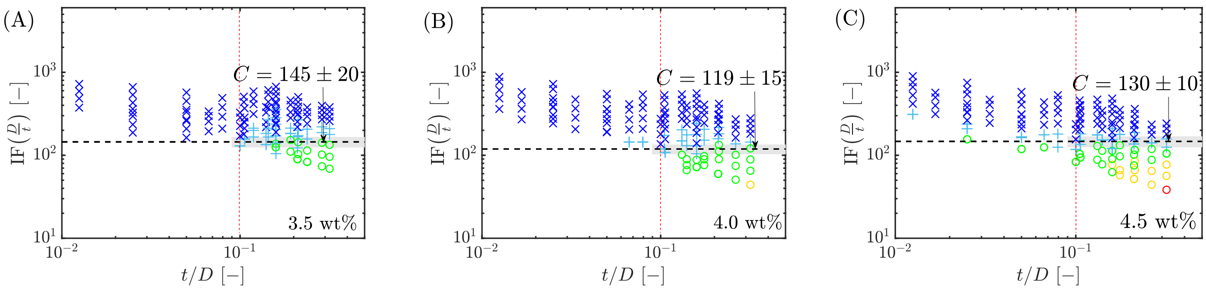

Figure S15: Full regime maps with the entire range of t/D used for Laponite.

9 Other dimensionless groups for comparing Laponite and Carbopol

In sec. 3.4 of the paper, we showed co-plots of Laponite and Carbopol impact data plotted as $\mathrm{IF}(D/t)$ vs. Bn. These were used to rationalise the difference in C values for the fluids. Other groups such as the Plastic number (Pl) and dimensionless consistency index (K^*), defined in the paper, can also be used to arrive at the same conclusions. Pl compares σ_y to the total shear stress, and is equivalent to using Bn ($\mathrm{Pl} = \mathrm{Bn}/(\mathrm{Bn}+1)$). K^* compares the power-law component of the shear stress to the total shear stress. These plots are shown in fig. S16.

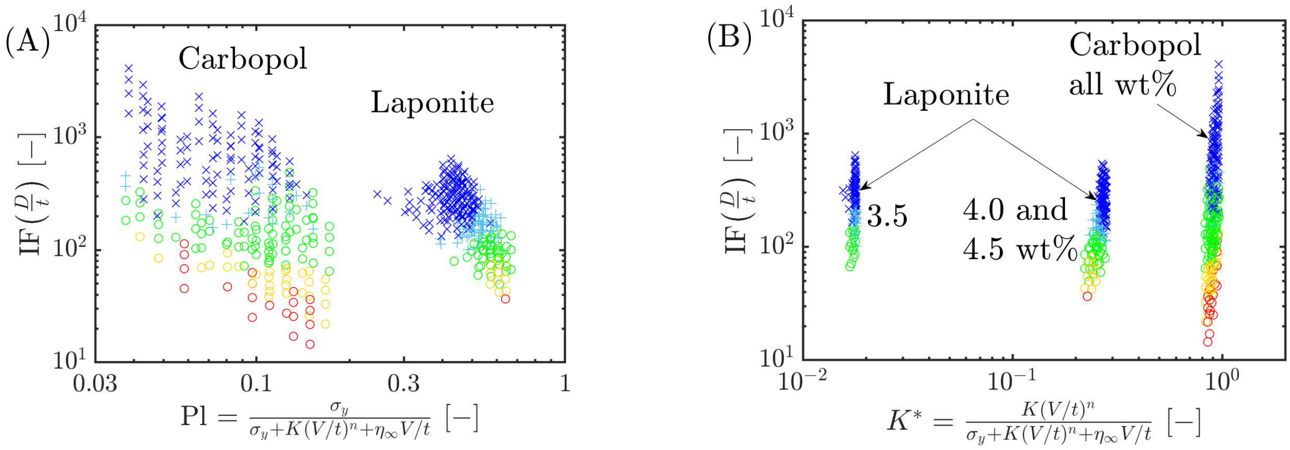

Figure S16: Co-plots of Laponite and Carbopol impact data plotted using (A) Pl and (B) K^*.

We clearly see that using Pl we observe the same trend as with Bn, and plots of K^* also corroborate the idea that plasticity effects are dominant in Laponite, while viscous stresses are more important for Carbopol. Note that in the plot of K^*, data for 3.5 wt% Laponite does not fall in the same region as 4.0 and 4.5 wt%. This is merely an artefact of the flow data and fitting models to it. From table S1, we see that the values of K are very small compared to η_∞ for 3.5 wt%, and this affects the plots of K^*.

References

[1] *Sticking and splashing in yield-stress fluid drop impacts on coated surfaces*, Blackwell, B.C., M.E. Deetjen, J.E. Gaudio, R.H. Ewoldt, Phys. Fluids 27, 043101 (2015)

[2] *Dynamics of Polymeric Liquids*, Bird, R.B., Armstrong, R.C., Hassager, O., Wiley, Vol. 1 (1987)

[3] *Experimental challenges of shear rheology with case studies in biological complex fluids, in: S.E. Spagnolie (Ed.)*, Ewoldt, R.H., M.T. Johnston, L.M. Caretta, Complex Fluids Biol. Syst., Springer, 207–241 (2015)

[4] *Quantitative rheological model selection: Good fits versus credible models using Bayesian inference*, Freund, J.B., R.H. Ewoldt, J. Rheol. 59, 667 (2015)

[5] *The impact of drops on walls and films*, Tropea, C., M. Marengo, Multiphase Sci. Technol. 11(1), 19–36 (1999)